analytical chemistry

Subscriber access provided by UCL Library Services

Article

Nanochannels Photoelectrochemical Biosensor

Nan Zhang, Yi-Fan Ruan, Li-Bin Zhang, Wei-Wei Zhao, Jing-Juan Xu, and Hong-Yuan Chen

Anal. Chem., **Just Accepted Manuscript** • DOI: 10.1021/acs.analchem.7b04862 • Publication Date (Web): 28 Dec 2017

Downloaded from http://pubs.acs.org on December 29, 2017

Just Accepted

"Just Accepted" manuscripts have been peer-reviewed and accepted for publication. They are posted online prior to technical editing, formatting for publication and author proofing. The American Chemical Society provides "Just Accepted" as a free service to the research community to expedite the dissemination of scientific material as soon as possible after acceptance. "Just Accepted" manuscripts appear in full in PDF format accompanied by an HTML abstract. "Just Accepted" manuscripts have been fully peer reviewed, but should not be considered the official version of record. They are accessible to all readers and citable by the Digital Object Identifier (DOI®). "Just Accepted" is an optional service offered to authors. Therefore, the "Just Accepted" Web site may not include all articles that will be published in the journal. After a manuscript is technically edited and formatted, it will be removed from the "Just Accepted" Web site and published as an ASAP article. Note that technical editing may introduce minor changes to the manuscript text and/or graphics which could affect content, and all legal disclaimers and ethical guidelines that apply to the journal pertain. ACS cannot be held responsible for errors or consequences arising from the use of information contained in these "Just Accepted" manuscripts.

ACS Publications

Analytical Chemistry is published by the American Chemical Society. 1155 Sixteenth Street N.W., Washington, DC 20036

Published by American Chemical Society. Copyright © American Chemical Society. However, no copyright claim is made to original U.S. Government works, or works produced by employees of any Commonwealth realm Crown government in the course of their duties.

Nanochannels Photoelectrochemical Biosensor

Nan Zhang[1,a], Yi-Fan Ruan[1,a], Li-Bin Zhang[1], Wei-Wei Zhao[1,2]*, Jing-Juan Xu[1]* and Hong-Yuan Chen[1]*

[1.] State Key Laboratory of Analytical Chemistry for Life Science and Collaborative Innovation Center of Chemistry for Life Science, School of Chemistry and Chemical Engineering, Nanjing University, Nanjing 210023, China

[2.] Department of Materials Science and Engineering, Stanford University, Stanford, California 94305, United States.

a.These authors contribute equally.

ABSTRACT: Nanochannels have brought new opportunities for biosensor development. Herein we present the novel concept of nanochannels photoelectrochemical (PEC) biosensor based on the integration of a unique Cu_xO nanopyramid islands (NPIs) photocathode, the anodic aluminum oxide (AAO) membrance, and the alkaline phosphatase (ALP) catalytic chemistry. The Cu_xO NPIs photocathode possessed good performance, and further assembly with AAO will yield the designed architecture composed of vertically-aligned, highly-ordered nanoarrays bottomed with Cu_xO NPIs film. With biocatalytic precipitation (BCP) stimulated within the channels, the biosensor was applied for the successful detection of ALP activity. This study has not only provided a novel paradigm for an unconventional nanochannels PEC biosensor that can be used for general bioanalytical purposes, but also indicated the new concept of nanochannels–semiconductor heterostructures as a step toward innovative biomedical applications.

One of the leading directions of state-of-the-art nanoscience and nanotechnology is focused on the development of novel nanostructures and their unique applications in manifold fields. Among numerous nanostructures, nanopores and nanochannels have emerged in the last decade as materials with versatile capabilities for various applications, including in electronics, energy conversion and storage, optoelectronic devices, nanofabrication and nanosensing.[1] Particularly, nanopores and nanochannels based sensing has recently drawn increasing attentions.[2] For example, the most widely used natural protein-based ion channels， i.e., the heptameric α-hemolysin bacterial protein pore from Staphilococus aureus, has been highly exploited for versatile sensing purposes.[3] Solid-state single nanochannels have also been fabricated by track-etching on polymeric membranes for biosensing.[4] Nanochannel arrays seem to bring different advantages for biosensor development and have been addressed for the detection of a variety of analytes.[5] Among them, anodic aluminum oxide (AAO) nanoporous membrane is beyond doubt the most popular nanochannel array.[6,7] It is of high interest in nanobiotechnology due to its stability, tissue compatibility, as well as high surface-to-volume ratio for increased guest immobilization. Its regular structure of well-ordered, hexagonal, honeycomb-like arrayed nanochannels with a narrow pore size distribution provides a well-defined, controllable, homogeneous interaction surface. The fabrication of AAO is simple and reproducible, and further increase or reduce the pore radius was also possible in highly controlled manners via the wet-chemical etching or the layer by layer (LbL) deposition of polymers, respectively. In addition to its versatile applications in catalysis,[8] energy,[9] electronics,[10] photonics[11] and etc., AAO has especially demonstrated itself as elegant platform for DNA, protein, small molecules, and bacteria biosensing with various optical (e.g., photoluminescence, (localized) surface-plasmon resonance, reflectometric interference spectroscopy) and electrical (e.g., voltammetry/amperometry, impedance, capacitance, resistivity/conductivity) modalities.[12-14]

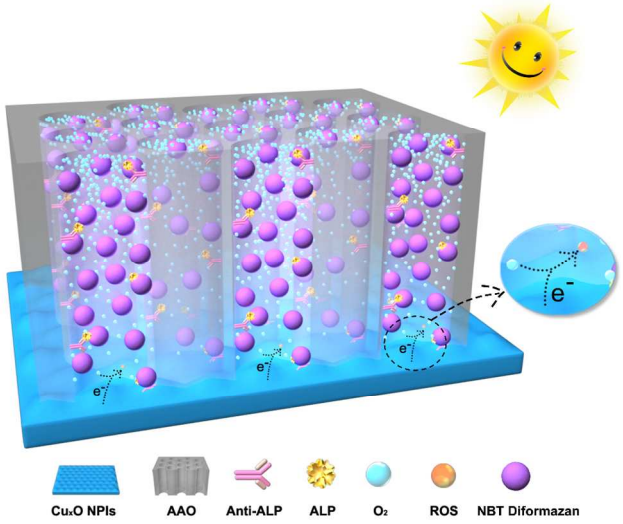

Scheme 1. Schematic illustration for AAO-based cathodic nanochannels PEC biosensor.

Photoelectrochemical (PEC) bioanalysis is a newly developed biomolecular detection technique which has promptly become a subject of hot research interest due to its desirable properties and attractive potential in future bioassays.[15-19] Basically, PEC bioanalysis is the advanced generation of electrochemical detection and it thus inherits the advantages of low

cost, robustness, fast responsibility and high sensitivity.[20-24] Besides, it operates with cheaper and simpler instrumentation as compared to various optical techniques.[25-28] To achieve efficient PEC bioanalysis, diverse functional nanostructures with innovative signalling mechanisms have been exploited for addressing various targets of interest. For example, recently, IrO_2−hemin−TiO_2 nanowire arrays,[29] N-doped carbon nanodot (N-Cdot)/TiO_2 nanowire,[30] hybrid organic/inorganic nanostructures,[31] mesoporous iron oxide nanopyramid islands (NPIs),[32] sandwiched Au nanoparticles (NPs)/reduced graphene oxide (RGO)/TiO_2 structure,[33] ZnO@ZIF-8 nanorods,[34] and periodically patterned Au nanorods in TiO_2 nanocavities[35] have been developed toward glutathione, cellular generation of H_2S, dissolved oxygen, H_2O_2, cell monitoring, and glucose, respectively. Despite these exciting progress, the possibility of nanopores and nanochannels in this promising field has not been unveiled.

Herein, we present the new concept of nanochannels PEC biosensor and demonstrate the proof-of-concept through a judiciously engineered PEC bionanosystem consisted of a unique Cu_xO NPIs photocathode, the nanoporous AAO membrane, as well as their synergistic combination with the alkaline phosphatase (ALP) catalytic chemistry. Specifically, as shown in Scheme 1, the Cu_xO NPIs photocathode was fabricated as the light-harvesting platform to accommodate the AAO membrane, yielding the designed structure of vertically-aligned, highly-ordered nanoarrays bottomed with Cu_xO NPIs film. With biocatalytic precipitation (BCP) within these tubes, this nanochannels PEC biosensor was then applied for detection of ALP activity, on the basis of the BCP-controlled photoresponses of the cathodic photocurrents. This study proposed a novel concept for an unconventional nanochannels PEC biosensor that can be extended for general bioanalytical purposes, and opens up a new perspective for using appropriately designed nanochannels (nanopores)-semiconductor heterostructures toward innovative biomedical applications, which to our knowledge has not been reported.

EXPERIEMENTAL SECTION

Materials and Apparatus. All chemical reagents were supplied from Sigma-Aldrich, Alfa Aesar, Nanjing Chemical Reagent Co., Ltd. and Sinopharm Chemical Reagent Co., Ltd, and were used without further purification. The ALP activity kit was from KeyGEN BioTECH (Cat. NO. KGT043). Ultrapure water (18.2 MΩ·cm resistivity at 25 °C, Millier Q) was used in all experiments. SEM images were recorded by a Hitachi S4800 scanning electron microscope (Hitachi Co., Japan). XPS was obtained from PHI 5000 VersaProbe (UlVAC-PHI Co., Japan). UV-vis absorption spectra and UV−vis diffuse reflectance spectra were obtained on a Shimadzu UV-3600 UV-vis-NIR spectrophotometer (Shimadzu Co., Japan). XRD spectra were characterized by powder X-ray diffraction (XRD, X'TRA, Cu Kα; ARL Co., Switzerland). PEC measurements were performed with a homemade PEC system equipped with a 5W light-emitting diode lamp with the emission wavelength of 410 nm. Photocurrent was measured on a CHI 660C electrochemical workstation (Chenhua, China) with a three-electrode system: a modified Cu_xO NPIs photocathode with a geometrical circular area (0.5 cm in diameter) as the working electrode, a Pt wire as the counter electrode and a saturated Ag/AgCl electrode as the reference electrode.

Synthesis of Cu_xO NPIs Photocathode. The Cu_xO NPIs photocathode was fabricated according to the previous reported method with modification[36]. Specifically, the FTO slices were cleaned by immersion in 2 M boiling KOH solution dissolved in 2-propanol for 15 min, followed by washing copiously with ethanol and ultrapure water, and dried under N_2. Cu film was deposited in a two electrode cell system using CHI 660C electrochemical work station as the power supply. Two slices of FTO glass were dipped into a saturated $CuSO_4$ solution with the conducting sides faced to each other and the Cu film was electrochemical deposited at the moderate rate of 100 mV s^{-1} in the potential regime of 0.0 V to 4.0 V for 30 segments at room temperature (one of the FTO glass working as both counter and reference electrode). Then the obtained Cu film was oxidized by annealing in a tube furnace for 4 h at 450 °C.

Immunoassay Development Carried on AAO Membrane. AAO membrane was washed by ethanol and ultrapure water in sequence to remove the impurities in the nanochannels. After drying under N_2, the AAO membrane was immersed into 1 mL of ethanol solution containing 5% APTES and kept at 4 □ overnight to generated amino groups on the surface and inside the channels. By shaking gently in ethanol for four times with 10 min each time, excess APTES was washed out. Then the AAO membrane was immersed into 1 mL of 50 μg/mL anti-ALP containing 5 mM EDC-NHS and left incubation for 16 h at 4 □, followed by washing with 10 mM PBS (pH=7.4) for four times to remove the physically absorbed antibodies. Then the membrane was blocked by 1 mL 3% BSA to avoid nonspecific absorption. After shaking in 10 mM PBS (pH=7.4) twice and 10 mM Tris-HCl (pH=8.0) twice, the sensing platform was built.

Detection of ALP Activity. In the detection process, ALP with different activity was reacted with the antibodies on the membrane for 2 h at 37 □, followed by washing in 10 mM Tris-HCl (pH=8.0) four times. Then the ALP-loaded membranes were immersed into 0.5 mL of commercially available BCIP/NBT solution for 30 min at 37 □, followed by washing with ultrapure water. AAO membrane was compactly fixed onto the conducting side of Cu_xO NPIs photocathode by physical attachment of a black gummed tape, with a circular working area of 5 mm in diameter. Another black gummed tape with a circular working area of 4 mm was stick onto the non-conducting side of the photoelectrode, forming concentric circles with the working area on the conducting side, allowing the irradiation light pass through. Then a PEC measurement was carried out with the light irradiating from backside.

RESULTS AND DISSCUSSION

Structural Information of Cu_xO NPIs. Experimentally, among various candidates, the Cu_xO, with direct band gap of 1.3~2.5 eV, was rationally selected due to its excellent balance in strong visible light responsibility, low cost, nontoxic, and especially, the photocathodic characteristics,[36,37] while NPIs nanostructure was utilized due to the distinct advantages as revealed in a recent report.[38] Figure 1a and 1b depicted the top and side views, respectively, of the morphology of as-

electrodeposited Cu_xO NPIs photocathode after annealing at 450 ℃ for 4 h by scanning electron microscope (SEM) images. As shown, the surface coverage of Cu_xO was substantially dense with many pyramid-like nanosized islands formed on the glass surface. X-ray photoelectron spectroscopy (XPS) characterization shown in Figure 1c offered direct insight into the chemical composition of the Cu_xO NPIs. The curve-fit results confirmed the co-existence of CuO (two peaks centered at 933.5 and 953.2 eV) and Cu_2O (two peaks centered at 932.4 and 952.2 eV). In addition, the effect of the annealing temperature on the composition change was also characterized by X-ray diffraction (XRD) with the results shown in Figure S1, and the color change of the electrode was also exhibited by a digital photograph in Figure S2.

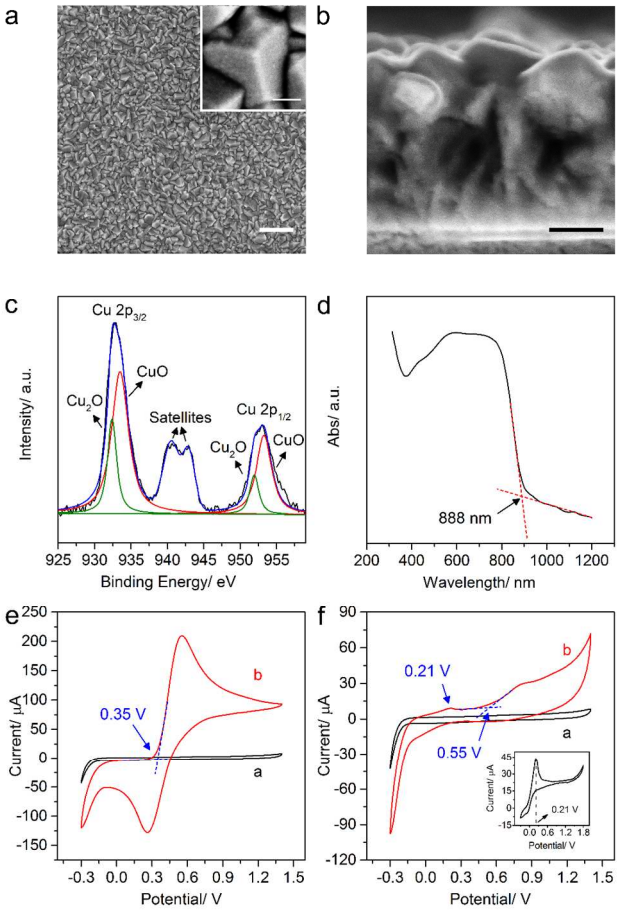

Figure 1. (a) SEM and (b) the cross-sectional view of the Cu_xO NPIs photocathode; the scale bar in 1a equaled to 1 μm and the rest equaled to 100 nm; (c) XPS spectra of the Cu 2p core level of Cu_xO NPIs; (d) UV-vis diffuse reflectance spectra of Cu_xO NPIs; The cyclic voltammogram of (e) FTO as working electrode in a deoxygenated anhydrous acetonitrile solution containing 0.1 M tetrabutylammonium hexafluorophosphate ($TBAPF_6$, curve a) and further containing 0.5 mM ferrocene (Fc, curve b) at a scan rate of 50 mV s^{-1}; (f) FTO (curve a), Cu_xO NPIs photocathode (curve b) and inset the Cu_2O electrode (obtained by annealing the electrodeposited Cu film at 250 ℃ for 4 h) as working electrode in 0.1 M $TBAPF_6$ solution respectively in the same condition.

To determine the energy gap (Eg) of this sample, UV-vis diffuse reflectance spectra of the photoelectrode was then performed with the result shown in Figure 1d. As recorded, the Cu_xO NPIs electrode exhibited an excellent light harvesting ability in a broad region from visible to near-infrared range, implying its suitability as a photoactive specie in PEC biosensor. The Eg was then calculated to be at a very small value of 1.40 eV by the cut-off wavelength of 888 nm, according to *Eq.* (1):

$$Eg\ (eV)=1240/\lambda_{cut\text{-}off}\ nm \qquad Eq.\ (1)$$

The specific energy levels of Cu_xO NPIs were further investigated by cyclic voltammetry (CV) according to bulk ionization potential (IP),[39,40] where a Pt wire worked as the counter electrode, a saturated Ag/AgCl as the reference electrode, and 0.1 M tetrabutylammonium-hexaflurophosphate ($TBAPF_6$) dissolved in acetonitrile as the electrolyte solution. The potential of Ag/AgCl was first calibrated by the oxidation potential of Fc/Fc^+ (-4.80 eV vs vacuum), herein located at 0.35 V, as shown in Figure 1e, therefore the potential of Ag/AgCl was calculated to be -4.45 eV vs vacuum. The valence band (VB) level of Cu_xO NPIs complied to *Eq.* (2), and the E_{VB} was calculated to be -5.00 eV using E_{ox} value of 0.55 V obtained from Figure 1f. E_{CB} was then calculated as -3.60 eV by *Eq.* (1) and *Eq.* (3),

$$E_{VB}= -IP = -(E_{ox}-I_{RE})\ eV \qquad Eq.\ (2)$$

$$E_{CB}= (E_{VB}+Eg)\ eV \qquad Eq.\ (3)$$

where E_{VB} and E_{CB} refers to the valence band and conduction band energy, E_{ox} equals the onset potential of the oxidation peak of Cu_xO NPIs, I_{RE} equals the absolute energy level to vacuum of the reference electrode, and Eg refers to the energy gap. Incidentally, the oxidation peak at 0.21 V was the oxidation process from Cu^{I} to Cu^{II}, since it agreed with the oxidation peak of pure Cu_2O electrode (obtained by annealing the as-electrodeposited Cu film at 250 ℃ for 4 h) in the same condition, shown in the Figure 1f inset. This results also confirmed the coexistence of Cu^{I} and Cu^{II} in the Cu_xO NPIs photocathode.

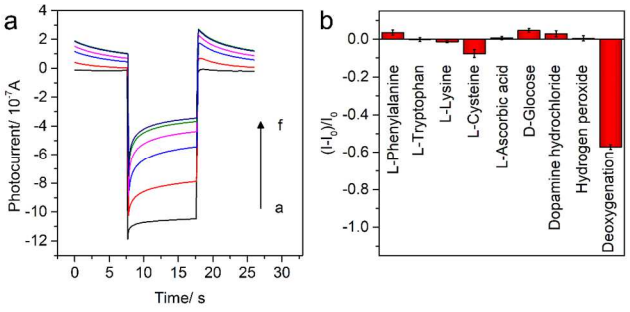

Figure 2. (a) the cathodic responses of the Cu_xO NPIs photocathode after deoxygenation with N_2 for 0, 1, 3, 5, 10, 30 min (from curve a to f); (b) Selectivity of the Cu_xO NPIs photocathode toward common interference species. I_0 is the photocurrent intensity measured in the air-saturated Tris-HCl solution (10 mM, pH 8.0), and I is the value after adding 10^{-4} M interfering reagents or deoxygenation with N_2 for 30 min. (Figure 2b has been updated)

PEC Properties of Cu_xO NPIs. Significantly, the obtained energy levels of Cu_xO NPIs implied that the electrode might be apt to react with the ambient oxygen (O_2) in the electrolyte solution. As shown in Figure S3, the band position of

Cu_xO, with respect to reactive oxygen species (ROS)-formation and O_2/H_2O potentials,[41] were calculated at the present condition and the results supported this assumption. To further validate this hypothesis experimentally, the chronoamperometric $I-t$ response of the as-fabricated Cu_xO NPIs electrode was recorded in Figure S4. As shown, a stable cathodic transient photocurrent over several cycles was observed upon the intermittent light irradiation in the air-saturated Tris-HCl solution (10 mM, pH 8.0), clearly demonstrating its favor for oxygen reduction reaction and the high stability of the electrode. The linear sweep photovoltammograms of the Cu_xO NPIs electrode, as shown in Figure S5, displayed the anti-dependence of the photocurrent with the bias potential, the essential characteristics of which conformed the as-fabricated Cu_xO NPIs as the p-type semiconductor.[42] To further study the feasibility of the Cu_xO photocathode in the proposed biosensor system, the sensitivity of this photocathode to ambient O_2 and the corresponding selectivity were then evaluated. When purged with highly pure nitrogen (N_2) to deoxygenated the solution, as manifested in Figure 2a, the photocurrent intensity gradually decreased with the duration of the purging time, indicating its intimate dependence on the amount of ambient dissolved O_2. Specifically, when the Cu_xO NPIs was excited by photons, electron/hole pairs was generated and separated to form the cathodic photocurrent due to the fast transfer of electrons towards the electrolyte than that of holes.[43] As the air-saturated electrolyte was deoxygenated by purging N_2, transfer of electrons to ambient O_2 would be inhibited along with enhanced recombination of the electron-hole pairs, resulting to a gradual inhibition of the cathodic photocurrent.[44,45] Especially, figure 2b disclosed the anti-interference property of the Cu_xO NPIs electrode. As shown, the electrode was totally independent to the common coexisting interfering species in biological fluids such as glucose, ascorbic acid, dopamine, hydrogen peroxide, amino acids and thio-compounds, further revealing the excellence of this electrode for subsequent application.

Nanochannels-based BCP Reaction. Next, anti-ALP were loaded within the AAO nanochannels for the subsequent specific capture of ALP, after which BCP was then introduced into the channels based on the efficient ALP catalytic chemistry. Figure S6 illustrated the specific catalyzed reaction process. In detail, during the enzyme catalysis, soluble 5-bromo-4-chloro-3-indolyl-phosphate (BCIP) and nitro-blue tetrazolium (NBT) will turn into insoluble dehydroindigo product and NBT diformazan, which was expected to accumulate on the surface and the inside channels of AAO. Obviously, the success of this process will cause the change of elemental proportion on the AAO surface, since elements such as C, N, Cl and Br will be brought in through the reaction. As shown in Figure S7 and Table S1, the energy dispersive X-Ray (EDX) composition analysis was then conducted for the 25 U/L ALP derived sample, and the increase of C, N, Cl and Br elements was recorded as expected. This phenomenon not only revealed the successful occurrence of BCP reaction, but also the good enzymatic activity after the bioaffinity recognition and confinement within the AAO channels.

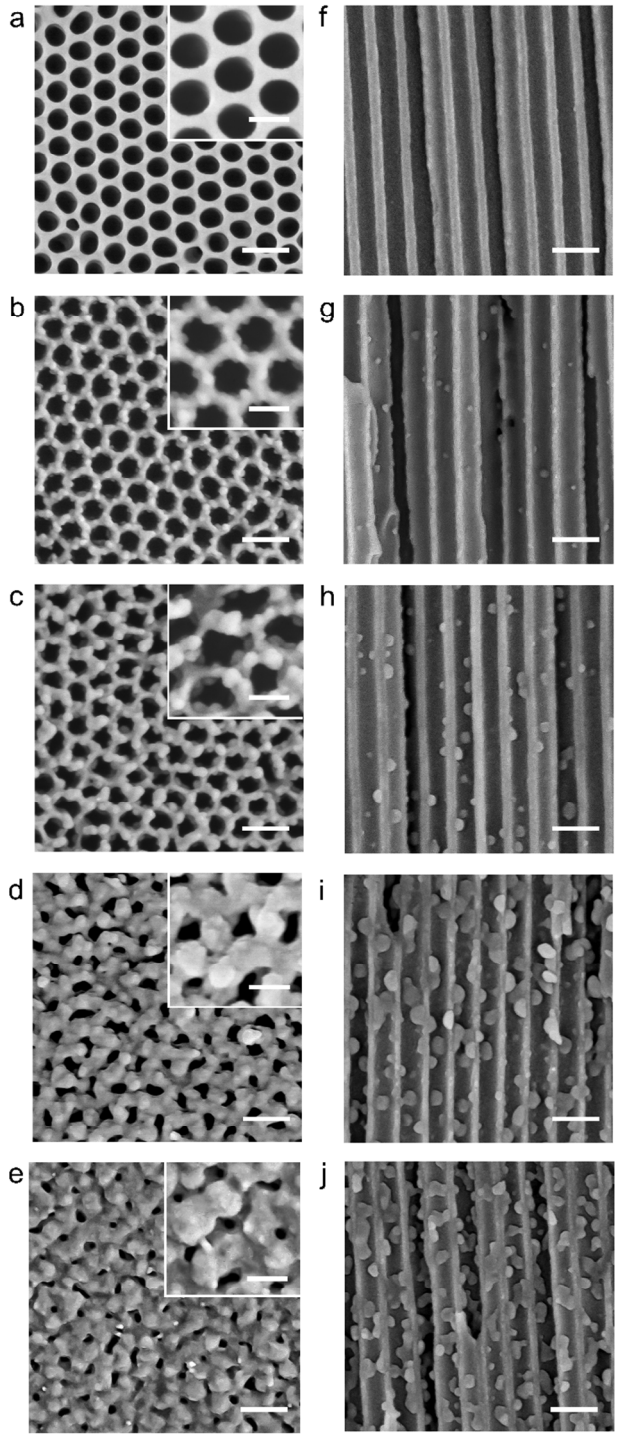

Figure 3. SEM (and inset HRSEM) images of the AAO membrane before and after BCP reaction in the presence of 0, 5, 10, 25, 40 U L^{-1} ALP, (a)-(e), respectively; and the corresponding cross section view, (f)-(j), respectively. The scale bars equal to 200 nm and the inset scale bars equal to 100 nm.

SEM characterization was then performed to unveil the details associated with the AAO during the BCP reaction corresponding to varying ALP activity. As shown in Figure 3, it is clear that the as-grown AAO film is composed of a self-organized honeycomb-like nanoporous structure in large scale

with a diameter of ca. 90 nm, and a uniform vertically-aligned nanochannels array could be observed from cross section view. This unique morphology obviously ensured an ultra-high specific surface area, which had a great potential for massive and regular biomolecular shipment. After ALP capture and the subsequent BCP reaction, nanosized particle-shape precipitation was found to deposit on the surface and within the channels. As the ALP activity increasing, the precipitation started to grow and accumulate and became more thick and dense. As shown, the hole opening on the surface was getting smaller while the internal was getting more crowded, blocking the nanochannels gradually. These results also in turn implied that the channels had been successfully employed for the uniform accommodation of the proteins (anti-ALP) and enzymes (ALP), and also its high biocompatibility for retaining these biomolecules. In addition, given that the precipitate was a bluish violet product,[46] we also found the incubation solution kept clear after the catalyzed reaction, demonstrating that the AAO was very good at enrichment of the precipitate. This made possible a convenient direct monitoring of the reaction process. As shown in Figure 4, a simultaneous color change, from semi-transparent white to dark purple, could be directly observed by naked eye. And a complementary colorimetric analysing could thus be built, on the basis of taking the color intensity as an index. Using the photographs, the corresponding value could be quantified in the blue channel with the help of Adobe Photoshop software, as illustrated in Figure S8.[47,48] Incidentally, we had also studied the pore size (ca. 280 nm) effect of the AAO film, and the results shown in Figure S9 demonstrated the suitability of 90 nm sample.

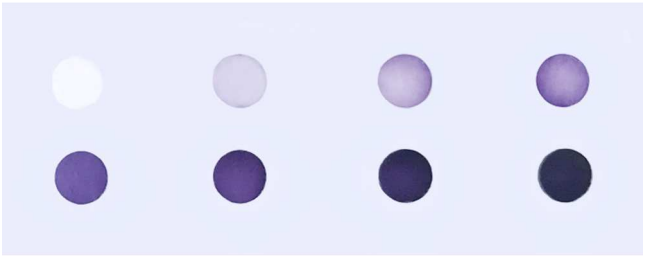

Figure 4. Digital photograph of AAO membrane before (the first one) and after BCP reaction in the presence of 1, 2.5, 4, 5, 10, 25, 40 U L^{-1} ALP, respectively.

Performance of the Nanochannels PEC Biosensor. Obviously, as the nanochannels gradually blocked, it will be more difficult for the solution solution-solubilized species (O_2) to diffuse within the clogged channels. Figure 5 depicted the performance of the proposed nanochannels PEC biosensor by simply recording the transient photocurrent that stimulated from the backside of the transparent FTO electrode. Figure 5a revealed the stepwise signal change as the biosensor development. As shown, upon light excitation, the bare Cu_xO NPIs promptly reached a steady cathodic photocurrent of 10.3×10^{-7} A (curve a). After accommodating AAO membrane, the absolute value of the photocurrent decreased to 8.44×10^{-7} A, due to the inherent impedance of AAO (curve b). The following modification of antibody-enzyme complex through silane chemistry only reduced the photocurrent slightly to 7.91×10^{-7} A (curve c), whereas this reduction is significantly magnified to 3.12×10^{-7} A after the BCP reaction corresponding to 10 U L^{-1} ALP (curve d). As shown in Figure 5b and 5c, with the activity of ALP increasing, the photocurrent kept decreasing. This result agreed well with the SEM and naked eye observation, i.e., the AAO channels acted not only as a substrate for biomolecular loading

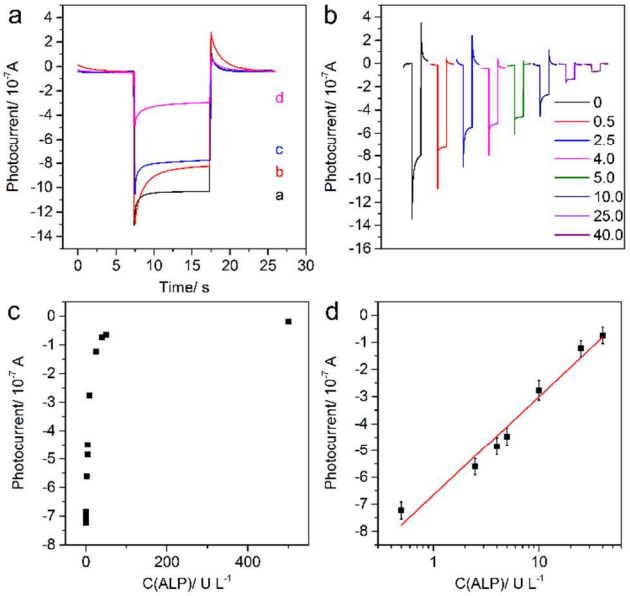

Figure 5. (a) Photocurrent response of (curve a) the bare Cu_xO NPIs photocathode, the electrode after (curve b) blank AAO membrane accommodation, (curve c) antibody-enzyme modification and (curve d) 10 U L^{-1} ALP catalyzed BCP reaction; (b) and (c) Photocurrent intensities after BCP reaction, corresponding to increased ALP activity; (d) The corresponding calibration curve.

and precipitation collecting, but also the important aisles connecting electrolyte and the photoelectrode. And then the BCP-induced deposition accumulated on the surface and inside the channels will block these aisles to a varying degree, thus introducing different steric hindrance against the diffusion of O_2 along the nanochannels to the Cu_xO NPIs electrode. The higher enzyme activity, the more severe signal inhibition will be caused. Figure 5d shows the corresponding derived calibration curve, demonstrating the linear correlation between the photocurrent intensity and the logarithm of ALP activity from 0.5 to 40.0 U L^{-1}, with a detection limit of 0.33 U L^{-1} (S/N = 3), and the linear equation was I (10^{-7} A) = 3.65 log (C_{ALP}, U L^{-1})-6.65, with a correlation coefficient R = 0.986. An interassay relative standard deviation (RSD) was used to evaluate the reproducibility. By analysing 10 U L^{-1} ALP with 5 electrodes, the RSD was calculated to be 8.5%, indicating acceptable reproducibility. Given the excellent anti-interference ability of the Cu_xO NPIs photocathode, the established linear equation in this protocol could be applied to determine the ALP activity in biological fluids, for example, diluted human serum. Actually, as a subfamily of phosphatase, ALP is of great importance in dephosphorylation process of proteins, DNAs and small molecules, whose disorder leads to the occurrence of several severe diseases such as dynamic bone disease, hepatitis, prostatic cancer and so on. The concentrations of ALP in healthy human blood is relatively low (ca. 40-120 U L^{-1}), and a significant elevation happens when there is liver, bone or other disease.[49,50] Accordingly, we then

determined the ALP activity in diluted healthy human serum by the proposed biosensor with the standard addition method, with the results presented in the Table S2. The coherence between our results and the commercial ALP kit results indicated that this protocol was qualified for applications in clinical diagnosis.

CONCLUSIONS

In summary, this work presented the new concept of nanochannels PEC biosensor and demonstrated the proof-of-concept through a judiciously engineered PEC bionanosystem consisted of a unique Cu_xO NPIs photocathode, the nanoporous AAO membrane, as well as their synergistic combination with the ALP catalytic chemistry. The as-fabricated Cu_xO NPIs photocathode possessed good performance in terms of strong and broad visible to near infrared light harvesting, fast generation of a stable cathodic photocurrent, and intrinsic anti-interference ability. The AAO nanochannel arrays acted simultaneously as a platform for protein loading, a vessel for biochemical reaction and product collecting, and also an aisle for solid-liquid interface connecting. With ALP-catalyzed precipitation reaction, we succeeded to analyze the ALP activity with a low detection limit in biological fluid, which was qualified for clinical use. This work not only featured the first use of a unique Cu_xO photocathode and nanochannels in PEC bioanalysis but also, upon the combination of various biorecognition events, provided a common basis for addressing of versatile targets. We further envision the new perspective of nanochannels–semiconductor heterostructures could pave the way for advanced biochemical devices with faster response, enhanced sensitivity and higher stability.

ASSOCIATED CONTENT

Supporting Information

The Supporting Information is available free of charge on the ACS Publications website at DOI: 10.1021/acs.analchem.xxxxx.

XRD of the annealed Cu film. Photographs, energy levels, photocurrent stability and linear sweep photovoltammograms of Cu_xO NPIs. EDX characterization and color intensity of the AAO membrane after ALP catalyze. Diameter optimization of the AAO membrane. Real sample analysis.

AUTHOR INFORMATION

Corresponding Author

*E-mail: zww@nju.edu.cn, zww@stanford.edu
* E-mail: xujj@nju.edu.cn
* E-mail: hychen@nju.edu.cn

Author Contributions

The manuscript was written through contributions of all authors. All authors have given approval to the final version of the manuscript.

ACKNOWLEDGMENT

Financial support from the National Natural Science Foundation of China (Grant nos. 21327902 and 21675080) and the Natural Science Funds of Jiangsu Province (Grant BK20170073) is appreciated. This work was also supported by a Project Funded by the Priority Academic Program Development of Jiangsu Higher Education Institutions.

REFERENCES

(1) Howorka, S. *Nat. Nanotechnol.* **2017**, *12*, 619-630.
(2) Martin, C. R.; Siwy, Z. S. *Science* **2007**, *317*, 331-332.
(3) Watanabe, R.; Soga, N.; Fujita, D.; Tabata, K. V.; Yamauchi, L.; Hyeon Kim, S.; Asanuma, D.; Kamiya, M.; Urano, Y.; Suga, H.; Noji, H. *Nat. Commun.* **2014**, *5*, 4519.
(4) Yameen, B.; Ali, M.; Neumann, R.; Ensinger, W.; Knoll, W.; Azzaroni, O. *Nano Lett.*. **2009**, *9*, 2788-2793.
(5) Eftekhari, F.; Escobedo, C.; Ferreira, J.; Duan, X.; Girotto, E. M.; Brolo, A. G.; Gordon, R.; Sinton, D. *Anal. Chem.* **2009**, *81*, 4308-4311.
(6) Md Jani, A. M.; Losic, D.; Voelcker, N. H. *Prog. Mater Sci.* **2013**, *58*, 636-704.
(7) Zhu, H.; Xu, Y.; Han, Y.; Chen, S.; Zhou, T.; Willander, M.; Cao, X.; Wang, Z. *Nano Research* **2015**, *8*, 3604-3611.
(8) Li, J.; Liu, Z.; Huang, G.; An, Z.; Chen, G.; Zhang, J.; Li, M.; Liu, R.; Mei, Y. *NPG Asia Mater.* **2014**, *6*, e94.
(9) Zhou, L.; Tan, Y.; Ji, D.; Zhu, B.; Zhang, P.; Xu, J.; Gan, Q.; Yu, Z.; Zhu, J. *Sci. Adv.* **2016**, *2*, e1501227.
(10) Huang, Y. C.; Chen, P. Y.; Huang, K. F.; Chuang, T. C.; Lin, H. H.; Chin, T. S.; Liu, R. S.; Lan, Y. W.; Chen, C. D.; Lai, C. H. *NPG Asia Mater.* **2014**, *6*, e85.
(11) Demchyshyn, S.; Roemer, J. M.; Groiß, H.; Heilbrunner, H.; Ulbricht, C.; Apaydin, D.; Böhm, A.; Rütt, U.; Bertram, F.; Hesser, G.; Scharber, M. C.; Sariciftci, N. S.; Nickel, B.; Bauer, S.; Głowacki, E. D.; Kaltenbrunner, M. *Sci. Adv.* **2017**, *3*, e1700738..
(12) Alvarez, S. D.; Li, C.-P.; Chiang, C. E.; Schuller, I. K.; Sailor, M. J. *ACS Nano* **2009**, *3*, 3301-3307.
(13) Liu, X.; Chen, L.; Liu, H.; Yang, G.; Zhang, P.; Han, D.; Wang, S.; Jiang, L. *NPG Asia Mater.* **2013**, *5*, e63.
(14) Santos, A.; Kumeria, T.; Losic, D. *TrAC, Trends Anal. Chem.* **2013**, *44*, 25-38.
(15) Zhao, W. W.; Xu, J. J.; Chen, H. Y. *Chem. Rev.* **2014**, *114*, 7421-7441.
(16) Zhao, W. W.; Xu, J. J.; Chen, H. Y. *Chem. Soc. Rev.* **2015**, *44*, 729-741.
(17) Zhao, W. W.; Wang, J.; Zhu, Y. C.; Xu, J. J.; Chen, H. Y.. *Anal. Chem.* **2015**, *87*, 9520-9531.
(18) Zhao, W. W.; Xu, J. J.; Chen, H. Y. *TrAC, Trends Anal. Chem.* **2016**, *82*, 307-315.
(19) Zhao, W. W.; Xu, J. J.; Chen, H. Y. *Anal. Chem.* **2018**, *90*, DOI: 10.1021/acs.analchem.7b04672
(20) Riedel, M.; Sabir, N.; Scheller, F. W.; Parak, W. J.; Lisdat, F. *Nanoscale* **2017**, *9*, 2814-2823.
(21) Li, L.; Zhang, Y.; Zhang, L.; Ge, S.; Liu, H.; Ren, N.; Yan, M.; Yu, J. *Anal. Chem.* **2016**, *88*, 5369-5377.
(22) Zeng, X.; Tu, W.; Li, J.; Bao, J.; Dai, Z. *ACS Appl. Mater. Inter.* **2014**, *6*, 16197-16203.
(23) Zhuang, J.; Tang, D.; Lai, W.; Xu, M.; Tang, D. *Anal. Chem.* **2015**, *87*, 9473-9480.
(24) Zhang, H.; Zhao, L.; Geng, F.; Guo, L.-H.; Wan, B.; Yang, Y. *Appl. Catal., B* **2016**, *180*, 656-662.
(25) Li, M.; Zheng, Y.; Liang, W.; Yuan, Y.; Chai, Y.; Yuan, R. *Chem. Commun.* **2016**, *52*, 8138-8141.
(26) Zhu, Y. C.; Zhang, N.; Ruan, Y. F.; Zhao, W. W.; Xu, J. J.; Chen, H. Y. *Anal. Chem.* **2016**, *88*, 5626-5630.
(27) Hao, N.; Zhang, X.; Zhou, Z.; Qian, J.; Liu, Q.; Chen, S.; Zhang, Y.; Wang, K. *Sens. Actuators, B* **2017**, *250*, 476-483.
(28) Hao, N.; Zhang, Y.; Zhong, H.; Zhou, Z.; Hua, R.; Qian, J.; Liu, Q.; Li, H.; Wang, K. *Anal. Chem.* **2017**, *89*, 10133-10136.
(29) Tang, J.; Kong, B.; Wang, Y.; Xu, M.; Wang, Y.; Wu, H.; Zheng, G. *Nano Lett.* **2013**, *13*, 5350-5354.

(30) Tang, J.; Zhang, Y.; Kong, B.; Wang, Y.; Da, P.; Li, J.; Elzatahry, A. A.; Zhao, D.; Gong, X.; Zheng, G. *Nano Lett.* **2014**, *14*, 2702-2708.
(31) Bellani, S.; Ghadirzadeh, A.; Meda, L.; Savoini, A.; Tacca, A.; Marra, G.; Meira, R.; Morgado, J.; Di Fonzo, F.; Antognazza, M. R. *Adv. Funct. Mater.* **2015**, *25*, 4531-4538.
(32) Kong, B.; Sikdar, D.; Tang, J.; Liu, Y.; Premaratne, M.; Zhang, W.; Jing, Y.; Zheng, G.; Selomulya, C.; Zhao, D. *NPG Asia Mater.* **2015**, *7*, e204.
(33) Xu, J. Q.; Liu, Y. L.; Wang, Q.; Duo, H. H.; Zhang, X. W.; Li, Y. T.; Huang, W. H. *Angew. Chem., Int. Ed. Engl.* **2015**, *54*, 14402-14406.
(34) Zhan, W. W.; Kuang, Q.; Zhou, J. Z.; Kong, X. J.; Xie, Z. X.; Zheng, L. S. *J. Am. Chem. Soc.* **2013**, *135*, 1926-1933.
(35) Guo, L.; Li, Z.; Marcus, K.; Navarro, S.; Liang, K.; Zhou, L.; Mani, P. D.; Florczyk, S. J.; Coffey, K. R.; Orlovskaya, N.; Sohn, Y. H.; Yang, Y. *ACS Sens.* **2017**, *2*, 621-625.
(36) Dubale, A. A.; Pan, C. J.; Tamirat, A. G.; Chen, H. M.; Su, W. N.; Chen, C. H.; Rick, J.; Ayele, D. W.; Aragaw, B. A.; Lee, J. F.; Yang, Y. W.; Hwang, B. J. *J. Mater. Chem. A* **2015**, *3*, 12482-12499.
(37) Paracchino, A.; Laporte, V.; Sivula, K.; Gratzel, M.; Thimsen, E. *Nat. Mater.* **2011**, *10*, 456-461.
(38) Kong, B.; Sikdar, D.; Tang, J.; Liu, Y.; Premaratne, M.; Zhang, W.; Jing, Y.; Zheng, G.; Selomulya, C.; Zhao, D. *NPG Asia Mater.* **2015**, *7*, e204.
(39) Dissanayake, D. M. N. M.; Lutz, T.; Curry, R. J.; Silva, S. R. P. *Appl. Phys. Lett.* **2008**, *93*, 043501.
(40) Muth, M.-A.; Carrasco-Orozco, M.; Thelakkat, M. *Adv. Funct. Mater.* **2011**, *21*, 4510-4518.
(41) Liu, C.; Kong, D.; Hsu, P. C.; Yuan, H.; Lee, H. W.; Liu, Y.; Wang, H.; Wang, S.; Yan, K.; Lin, D.; Maraccini, P. A.; Parker, K. M.; Boehm, A. B.; Cui, Y. *Nat. Nanotechnol.* **2016**, *11*, 1098-1104.
(42) Dai, P.; Li, W.; Xie, J.; He, Y.; Thorne, J.; McMahon, G.; Zhan, J.; Wang, D. *Angew. Chem., Int. Ed. Engl.* **2014**, *53*, 13493-13497.
(43) Choudhary, S.; Upadhyay, S.; Kumar, P.; Singh, N.; Satsangi, V. R.; Shrivastav, R.; Dass, S. *Int. J. Hydrogen Energy* **2012**, *37*, 18713-18730.
(44) Wang, G. L.; Shu, J. X.; Dong, Y. M.; Wu, X. M.; Zhao, W. W.; Xu, J. J.; Chen, H. Y. *Anal. Chem.* **2015**, *87*, 2892-2900.
(45) Dai, W. X.; Zhang, L.; Zhao, W. W.; Yu, X. D.; Xu, J. J.; Chen, H. Y. *Anal. Chem.* **2017**, *89*, 8070-8078.
(46) Vella, S. J.; Beattie, P.; Cademartiri, R.; Laromaine, A.; Martinez, A. W.; Phillips, S. T.; Mirica, K. A.; Whitesides, G. M. *Anal. Chem.* **2012**, *84*, 2883-2891.
(47) Wang, P.; Lei, J.; Su, M.; Liu, Y.; Hao, Q.; Ju, H. *Anal. Chem.* **2013**, *85*, 8735-8740.
(48) Zhang, N.; Ruan, Y. F.; Ma, Z. Y.; Zhao, W. W.; Xu, J. J.; Chen, H. Y. *Biosens. Bioelectron.* **2016**, *85*, 294-299.
(49) Jin, L. Y.; Dong, Y. M.; Wu, X. M.; Cao, G. X.; Wang, G. L. *Anal. Chem.* **2015**, *87*, 10429-10436.
(50) Tan, Y.; Zhang, L.; Man, K. H.; Peltier, R.; Chen, G.; Zhang, H.; Zhou, L.; Wang, F.; Ho, D.; Yao, S. Q.; Hu, Y.; Sun, H. *ACS Appl. Mater. Inter.* **2017**, *9*, 6796-6803.

For TOC only